IEEE Photonics Journal
An IEEE Photonics Society Publication

Open Access

Symmetrical Emission Transparent Organic Light-Emitting Diodes With Ultrathin Ag Electrodes

Volume 10, Number 3, June 2018

Illhwan Lee
Sungjun Kim
Jae Yong Park
Sungjoo Kim
Hyung Won Cho
Juyoung Ham
Seungo Gim
Kisoo Kim
Kihyon Hong
Jong-Lam Lee

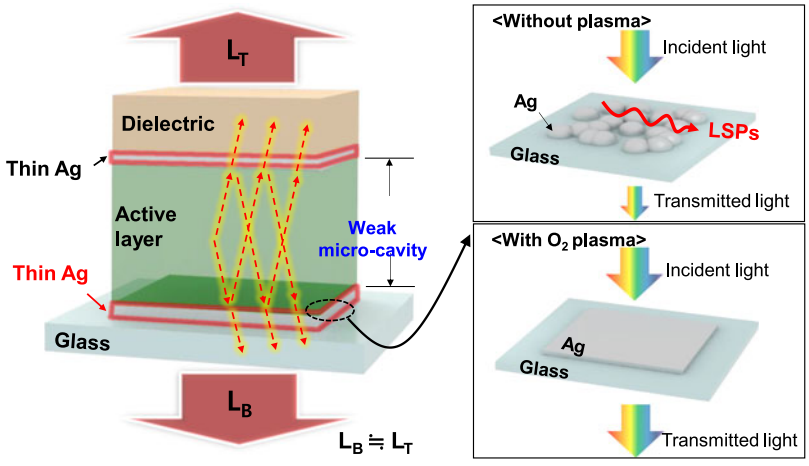

DOI: 10.1109/JPHOT.2018.2823759
1943-0655 © 2018 IEEE

IEEE photonics SOCIETY

IEEE

Symmetrical Emission Transparent Organic Light-Emitting Diodes With Ultrathin Ag Electrodes

Illhwan Lee,[1] Sungjun Kim,[1] Jae Yong Park,[1] Sungjoo Kim,[1] Hyung Won Cho,[1] Juyoung Ham,[1] Seungo Gim,[1] Kisoo Kim,[1] Kihyon Hong,[1] and Jong-Lam Lee [1, 2]

[1]Department of Materials Science and Engineering, Pohang University of Science and Technology, Pohang 790-784, South Korea
[2]Division of Advanced Materials Science, Pohang University of Science and Technology, Pohang 790-784, South Korea

DOI:10.1109/JPHOT.2018.2823759
1943-0655 © 2018 IEEE. Translations and content mining are permitted for academic research only. Personal use is also permitted, but republication/redistribution requires IEEE permission. See http://www.ieee.org/publications_standards/publications/rights/index.html for more information.

Manuscript received December 26, 2017; revised March 26, 2018; accepted March 28, 2018. Date of publication April 6, 2018; date of current version May 11, 2018. This work was supported by the National Research Foundation of Korea (NRF) grant funded by the Korea Government Ministry of Science, ICT and Future Planning (MSIP) under Grants NRF-2013R1A2A2A01069237 and NRF-2014H1A2A1021655-Global Ph.D. Fellowship program. The authors also would like to acknowlede for support from POSCO. Corresponding authors: Jong-Lam Lee and Kihyun Hong (e-mail: jllee@postech.ac.kr and khong@cnu.ac.kr).
Prof. K. Hong, Present Adress: Department of Materials Science and Engineering, Chungnam National University, Daejeon 34134, South Korea.
This paper has supplementary downloadable material available at http://ieeexplore.ieee.org.

Abstract: This paper describes a way to implement a transparent electrode for symmetrical emission from the bottom and top sides of transparent organic light-emitting diodes (TOLEDs). An ultrathin (~6 nm) and smooth Ag film was achieved by using the pretreatment of using oxygen plasma prior to deposition of a nanoscale-thin Ag film on glass. The treatment increased the surface energy, thereby enhancing the wettability of the Ag on glass substrate and consequently leading to the formation of thin and unifrom Ag film with high optical transmittance $T \sim 76\%$ and low sheet resistance $R_S < 15\ \Omega\ \square^{-1}$. Using this scheme, a highly transparent glass/Ag/WO_3 structure with $T = 85.6\%$, and $R_S = 9.3\ \Omega\ \square^{-1}$ was designed (ITO: 83.1%, 10 $\Omega\ \square^{-1}$). We conducted finite-domain time-difference simulation for this glass/Ag/WO_3 electrode to design a weak microcavity structure that retained the transparency and emitting properties. This optimized structure of TOLEDs (Ag = 6 nm) showed higher $T = 73.84\%$ than those of ITO devices ($T = 73.19\%$), and can induce the weak microcavity effect, resuting in improved electroluminescent properties and increased the luminance value from 38.25 to 56.25 cd A^{-1} at 25 mA cm^{-2}.

Index Terms: Organic light-emitting diode, transparent, ultra-thin, bi-directional, micro-cavity.

1. Introduction

Transparent organic light-emitting diodes (TOLEDs) can open new applications for bi-directional displays, transparent displays, wearable displays, smart glass, and window lighting [1]–[5] Early studies on TOLEDs used transparent conducting oxides (TCOs) such as indium tin oxide (ITO) and aluminum zinc oxide (AZO) for both the cathode and anode [6], [7]. Typically, these TCO films are obtained using sputtering techniques, which can significantly damage the underlying organic

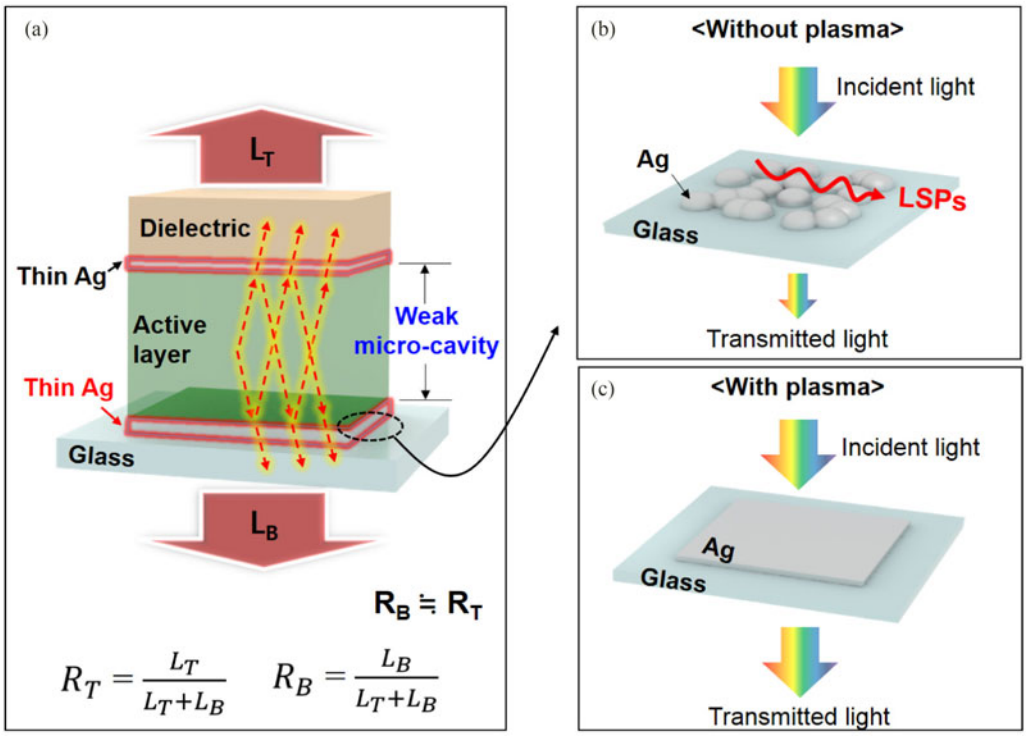

Fig. 1. (a) Schematic explanation of nanoscale thin Ag based TOLEDs. Schematic illustration of dewetting of Ag on glass substrate (right-top) and wetting of Ag on glass substrate (right-bottom).

layers, leading to the degradation of light emitting performance [8], [9]. To protect the underlying organic layer from sputtering damage, a thin metal-based semi-transparent cathode such as Ca, Al, and Ag can be prepared by thermal evaporation. Thus, to realize practical applications, the device structure of TOLEDs must consist of an ITO bottom anode, an emitting layer, and a thin Ag top cathode [10]. However, use of transparent ITO and semi-transparent thin Ag electrode for TOLEDs encounters three main drawbacks (Table S1 [7], [11]–[24]). First, these TOLEDs usually have preferential one-sided emission due to differences in reflection between ITO and Ag electrodes [11]–[14]. In particular, the bottom-side (ITO-side) emission R_B has a strong intensity which is $>70\%$ of the total emission R_T (R_B + top − side emission) because of the relatively low reflection of ITO compared with Ag film [see Fig. 1(a)]. This asymmetric emission property is not appropriate for bi-directional displays and lighting. Second, thin Ag-based TOLEDs have low optical transparency, T. Theoretically, thin Ag film with thickness below 10 nm can show high optical transmittance due to its low refractive index n and high extinction coefficient k [25]. However, Ag layers exhibit three-dimensional (3D) island growth mode during physical deposition process as a result of the poor wettability of Ag on the substrate [see Fig. 1(b)]. Ag has a high surface energy ($1.25\,\mathrm{Jm}^{-2}$) compared to that of the glass substrate ($0.06\,\mathrm{Jm}^{-2}$) [26]. This means that the Ag atoms interact more strongly with each other than with the glass substrate. This 3D island growth mode at the initial stage of film growth causes a significant delay in the formation of continuous Ag film [27], [28]. Thus, a discrete Ag thin film that consist of islands strongly absorbs and scatters light due to localized surface plasmon resonance (LSPR) [29]–[31]. To obtain a conductive and transparent Ag film, it must be continuous and smooth [32]. Wetting of Ag layer on the substrate can be significantly improved by adding seed materials such as Au, Al, Ca, Ge, Ni, MoO_3, or Cs_2CO_3 [33]–[37]. A seed layer reduces the difference in surface energy between the substrate and Ag. However, as a result of inserting seed materials, the T of film decreased. Among various metals, Ag has the lowest light adsorption in visible wavelength due to its low values of n and k (Fig. S1). Therefore, to obtain highly transparent Ag electrodes, a seed-free Ag wetting method is mandatory. Third, the efficiency

of TOLEDs must be increased. Most of the light generated in the organic layers is confined in the ITO ($n_{ITO} = 1.9$) anode and glass ($n_{glass} = 1.5$) substrates due to the large difference in the refractive index of each layer. This light trapping reduces the out-coupling efficiencies to only ~20% due to the total internal reflection at the ITO / glass and glass / air interfaces (waveguide mode) [38]. Most effective approaches to reduce light trapping (increase light extraction) in TOLEDs are based on micro-cavity effects by using an Ag cathode with Ag thickness $T_{Ag} > 10$ nm [15]–[17], [39]. Although micro-cavity effects can increase the extraction efficiency, the device's T is degraded due to reflection by the electrodes [17]–[19]. Such problems could be solved ultra-thin Ag electrodes on both the top and bottom transparent electrodes with O_2 plasma treatment on the glass and careful design of the weak micro-cavity structure. The O_2 plasma treatment allows deposition of a continuous ultra-thin Ag film with high T and low sheet resistance [40], [41]. The careful design of both the top and bottom Ag transparent electrodes enables symmetrical bi-directional displays by preventing preferential one-sided emission.

Here, we demonstrate an innovative method to make transparent and high performance OLEDs on glass substrates using only ultra-thin Ag electrodes on both the top and bottom transparent electrodes. We show that O_2 plasma treatment of the glass for only 1 min before deposition of the Ag layer leads to significantly improved homogeneity of the Ag layer [see Fig. 1(c)]. O_2 plasma treatment allows deposition of a continuous ultra-thin Ag film, thereby leading to $T > 70\%$ and sheet resistance $R_S < 15\,\Omega\,\square^{-1}$. Careful design of the weak micro-cavity structure with the ultra-thin Ag electrodes reduced waveguide modes increased the T of TOLEDs, and their luminance from 38.25 cd A^{-1} to 56.25 cd A^{-1} at 25 mA cm^{-2}. The TOLED with the ultra-thin Ag electrode showed $T = 73.84\%$, which is similar to that of ITO device (73.19%).

2. Experimental Details

Device fabrication: TOLEDs with nanoscale thin Ag electrodes were fabricated on glass substrate. The surface of the glass was cleaned in sequence with acetone, iso-propyl alcohol and deionized water, and then dried with high-purity N_2 gas. After the cleaning process, the substrates were loaded into a treatment chamber, then exposed to O_2 ambient at a partial pressure of 100 mTorr. The plasma was created using an RF generator operating at an output power of 50, 150 or 250 W. The substrates were loaded into the treatment chamber, then Ag (5, 6, 7, 9 nm), WO_3 30 nm, WO_3-doped 4,4'-N,N'-dicarbazole-biphenyl (CBP) 32 nm, Tris[2-phenylpyridinato-C2, N]iridium(III) ($Irppy_3$)-doped CBP 23 nm, 1, 3, 5-Tris(1-phenyl-1H-benzimidazol-2-yl)benzene (TPBi) 35 nm, LiF 1 nm, Al/Ag 0.5 nm/7 nm and CBP 62 nm were deposited in sequence as a hole injection layer (HIL), hole transport layer (HTL), emissive layer (EML), electron transporting layer (ETL), electron injection layer (EIL), semi-transparent cathode and capping layer respectively. Each layer was deposited with appropriate shadow masks and the active area was defined to be 4 mm^2. For reliable values, the OLEDs was fabricated repeatedly at least three times.

Simulation: Commercial software (The Essential Macleod, Thin Film Center, Inc.) based on what is known as the characteristic matrix method was used for optical analysis involving a multilayer structure. The 2D finite domain time-difference method with a PML was used in numerical analysis of the light extraction efficiency and electric field distribution. The optical constants of Ag, CBP, TPBi and WO_3 were measured by spectroscopic ellipsometry and taken from the literature. The simulation structure consists of a CBP capping layer ($n = 1.75$) 62 nm, Ag cathode (7 nm), Aluminum 0.5 nm, LiF (refractive index $n = 1.39$) 1 nm, TBPi ($n = 1.75$) 35 nm, CBP:$Ir(ppy)_3$ ($n = 1.75$) 18 nm, CBP ($n = 1.75$) 5 nm, CBP:WO_3 ($n = 1.77$) 32 nm, WO_3 ($n = 1.92$) 3 nm, ITO ($n = 1.96$) 170 nm or Ag 4 ~ 10 nm, and a glass substrate ($n = 1.5$) 3 μm (Fig. S9). The refractive index (n) and extinction coefficient (k) of Ag were plotted in Fig. S10.

Measurement and characterization: Both Ag and WO_3 were prepared by thermal evaporation on a glass substrate. The films were grown at a rate of 3 $Å s^{-1}$ under a base pressure of ~10^{-6} mTorr. The integrating sphere transmittance of Ag samples were recorded at $400 \leq \lambda \leq 700$ nm using an Agilent Technologies Cary 4000 UV-Vis spectrometer. The scattering images and spectra of the Ag samples were measured using a dark-field microscopy with a true color imaging change-coupled

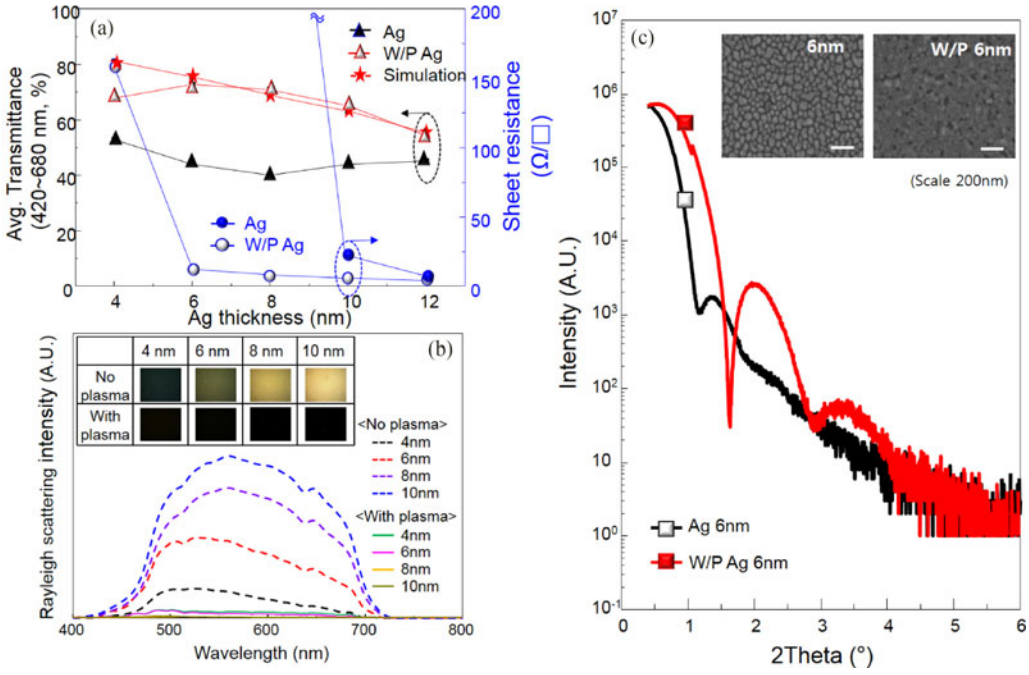

Fig. 2. (a) Calculated values and measured values of transmittance integrated from a wavelength of 420 to 680 nm and sheet resistance of glass/Ag without plasma and with oxygen plasma as a function of Ag thickness. (b) Rayleigh scattering spectra of glass/Ag without plasma and with oxygen plasma and dark-field reflection images of glass/Ag (inset). (c) X-ray reflectivity spectra for as-received glass/Ag 6 nm and plasma treated glass/Ag 6 nm. SEM images of as-received and plasma treated glass/Ag 6 nm samples (Inset, scale bar: 200 nm).

device (CCD) camera and a spectrometer. The sheet resistance of thin Ag film was measured with a 4-point probe geometry with 1 mm distance between the probes and Keithley 2400 source meter. The sheet resistance was measured repeatedly at least 5 times and the values were averaged. The Scanning Electron Microscopy (SEM) was used a PHILIPS XL30S with an accelerating voltage of 10 kV and a working distance of 6 mm. X-ray reflectivity (XRR) measurement was performed using Cu K_α radiation (Bruker).

3. Results

3.1 Formation of Ultrathin Ag Film

We measured R_S and average T ($420 \leq \lambda \leq 680$ nm) of Ag film on the as-received and plasma-treated glass substrates as a function of Ag thickness [T_{Ag}, Fig. 2(a)]. In the as-received glass, R_S was infinite at $T_{Ag} < 10$ nm due to island growth of the Ag film. However, the Ag on the glass treated with 250-W plasma did not form islands and yielded a continuous Ag film. Plasma treatment decreased R_S ($<15\,\Omega\,\square^{-1}$) even in the thin Ag film (6 nm). In the spectral range $420 \leq \lambda \leq 680$ nm, the as-received glass/Ag films had $T < 60\%$, but the plasma-treated glass/Ag films had $T = 70\%$ due to suppression of LSPR losses caused by growth of 3D Ag islands. For the $T_{Ag} = 6$ nm sample (plasma power $>$ 150 W, process pressure 100 mTorr), measured T agreed well with simulated T [see Fig. S2(c)].

We also obtained dark-field reflectance images (see Fig. 2) of glass/Ag film samples that had been or had not been plasma-treated. The brightness of dark-field images seen in the without plasma treated glass/Ag film samples due to collection of the scattered light by LSPR (see Fig. 2(b), inset). To further investigate the LSPR of the Ag in each sample, we also measured detailed scattering profiles [see Fig. 2(b)]. In the plasma-untreated samples, the spectra had high intensity and showed

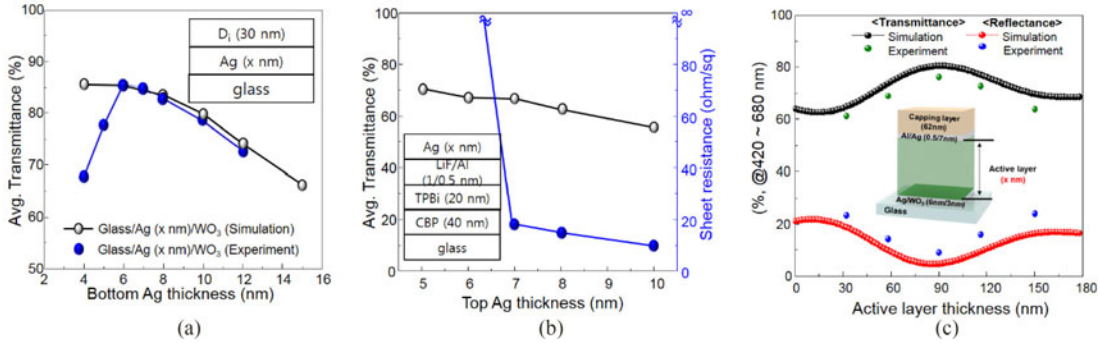

Fig. 3. (a) Calculated value (black line) and measured value (blue line) of transmittance integrated from a wavelength of 420 to 680 nm for bottom electrode (glass/Ag/WO_3) as a function of Ag thickness. (b) Transmittance and sheet resistance of top electrode (glass/CBP/TPBi/LiF/Al/Ag) as a function of Ag thickness. (c) Calculated average reflection and transmittance as a function of active layer thickness. Green and blue dots are measured value.

with the LSPR signature at $450 \leq \lambda \leq 700$ nm. However, the plasma-treated glass/Ag samples had no specific peaks related to LSPR. This result demonstrates that O_2 plasma treatment suppresses LSPR. X-ray reflectivity (XRR) measurements were acquired to measure the roughness of ultra-thin Ag film. In the reflectivity curves [see Fig. 2(c)] the oscillation in the reflected X-ray intensity was sharper, had higher modulation, and was more pronounced in reciprocal space for the plasma-treated sample than for the as-received sample. XRR intensity decreases rapidly in reciprocal space as interfacial roughness increases, so the observed interference fringes and oscillations present in the spectra of the plasma-treated sample clearly indicate that its surface was smoother and had less interface roughness than did the as-received sample [42]. The as-received glass/Ag sample tended to form islands (see Fig. 2(c), inset). These islands are not part of a charge-carrier percolation network, so they hinder charge movement. This problem can be solved by treating the glass with O_2 plasma before deposition of Ag film. O_2 plasma treatment increased the surface energy of glass substrate (see Fig. S3). This means that O_2 plasma treatment reduced the difference in surface energy between the substrate and Ag. Therefore, Ag atoms tend to form a continuous film on the substrate. O_2 plasma treatment was used to change the growth mode of the Ag film. This treatment to the glass can be used to optimize the growth of the evaporated Ag film, and thus obtain smooth and homogeneous layers, even if the total thickness of the metal layer is $<$10 nm (see Fig. S4).

3.2 Design of Ultrathin Ag Based TOLED

To empoly thin Ag film into TOLEDs as a bottom electrode, we used dielectric (D_i)/Ag/dielectric (D_o) structure. The WO_3 was chosen for D_i and D_o, because its high work function ($>$4.8 eV) for hole injection. In addtion, the WO_3 has high refractive index, $n = 1.9$, thus the combination of WO_3 and thin Ag film can result in high transmittance of electrode. First, we fixed a 30-nm-thick inner WO_3 (D_i) hole injection layer. To find the optimum thickness of the Ag and outer WO_3 (D_o) layers, we simulated a contour plot (see Fig. S5) of transmittance ($400 \leq \lambda \leq 700$ nm) for glass/D_o/Ag/D_i as a function of various Ag and D_o thickness. The optical simulation was performed using characteristic matrix theory [43]. Our simulation results suggested that using a D_o film as an antireflection layer may increase the T of a layer with $T_{Ag} > 10$ nm. However, the effect of the D_o layer is negligible when $T_{Ag} < 10$ nm because the T of glass/Ag/D_i structure is highest without D_o. The simulation showed that glass/Ag ($<$ 10 nm)/ D_i structure is suitable for obtaining a 'zero reflection' condition (see Fig. S6). We compared simulated and measured bottom electrodes transmittance of the glass/Ag/D_i ($T_{Ag} =$ x nm, $D_i = 30$ nm) as a function of various bottom Ag thicknesses [see Fig. 3(a)]. To obtain continuous ultra-thin Ag, the glass was treated by the O_2 plasma before deposition of Ag film. Both Ts were averaged in the visible wavelength ($400 \leq \lambda \leq 700$ nm). For Ag samples that

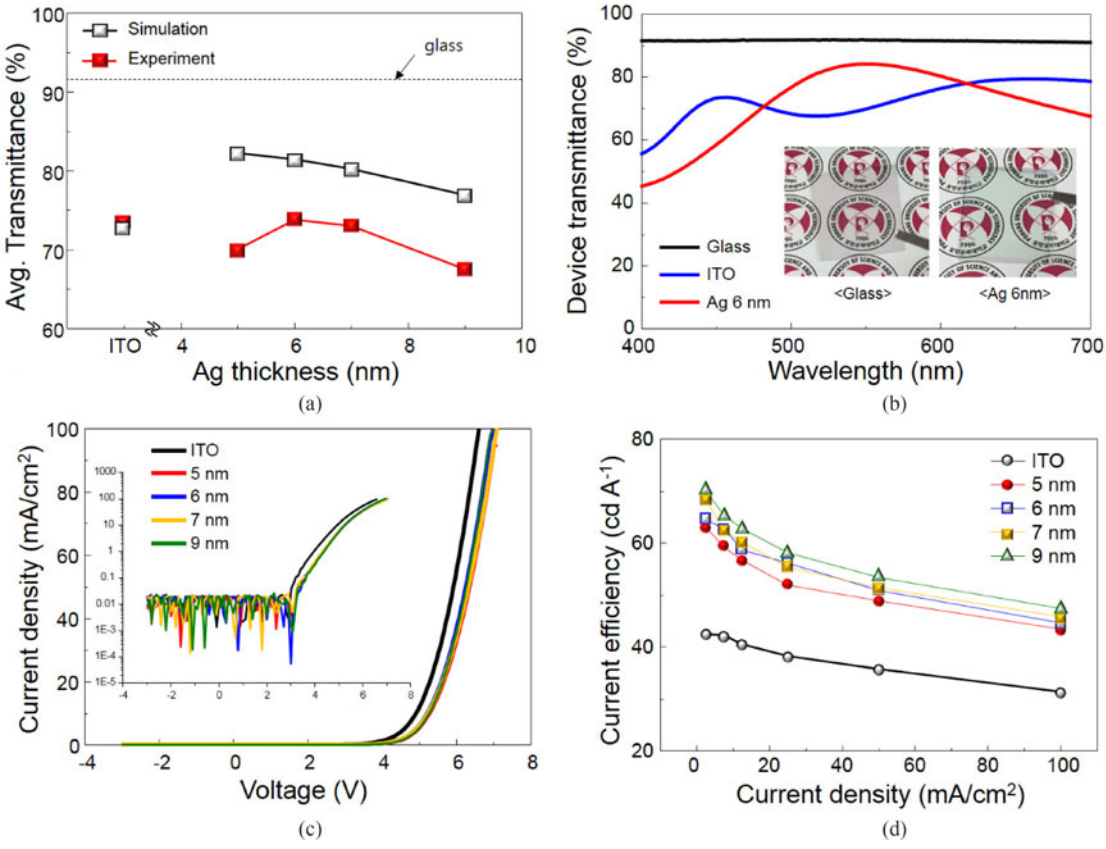

Fig. 4. (a) Calculated value (black) and measured value (red) of transmittance integrated from wavelength of 420 to 680 nm for glass/Ag based TOLEDs as a function of Ag thickness. (b) Transmittance spectrum of ITO and Ag based TOLEDs. The insets are the corresponding photographs. (c) Current density-voltage characteristics of TOLEDs as a function of Ag thickness. (d) Current density of TOLEDs vs. current efficiency.

had $T_{Ag} = 4$ nm and $T_{Ag} = 5$ nm, the simulated T was higher than the measured T; this difference is originated from the Ag agglomeration, which leads to LSPR. Ag samples with $T_{Ag} = 6$ nm had the highest T (85.6%) of all samples. The T of the glass/CBP (40 nm)/TPBi (20 nm)/LiF (1 nm)/Al (0.5 nm)/Ag samples decreased linearly as T_{Ag} increased [see Fig. 3(b)]. We used a thin Al seed layer to increase the surface energy, thereby increasing the wettability of the Ag and to high $T \sim$ 66.8% and low $R_S < 18\,\Omega\,\square^{-1}$ of the Ag film [44]. We designed a device structure in which the thicknesses of the active layer were optimized optically to achieve weak micro-cavity structure while maintaining optimal top and bottom Ag thickness (top Ag: 7 nm, bottom Ag: 6 nm). According to the Fabry-Perot principle, the reflection spectrum of the device dips at the resonance wavelength [45]. The calculated average reflection and T matches well with the broad dip in the reflection at 90-nm-thick active layer [see Fig. 3(c)], and the 90-nm-thick active layer had the highest T, because the destructive interference of the weak micro-cavity reduced the internal reflection of TOLEDs. This observation means that the weak micro-cavity structure of TOLEDs could increase both the device's out-coupling efficiency and T.

3.3 Device Performance of TOLEDs

Simulated average T ($420 \leq \lambda \leq 680$ nm) of the TOLEDs was higher than measured T [see Fig. 4(a)]. As T_{Ag} decreased, simulated T increased linearly whereas measured T increased only

until $T_{Ag} = 6$ nm (73.84%), and decreased at $T_{Ag} = 5$ nm due to the island growth of Ag film at initial stage , which led to LSPR absorption. The decrease in measured T at $T_{Ag} > 6$ nm occurred due to reflection of light by Ag and this result is in well agreement with the optical properties of our electrode structure in Fig. 3(a). In the transmittance spectra [see Fig. 4(b)] and photographs (see Fig. 4(b), insets) of TOLEDs, the device with $T_{Ag} = 6$ nm showed T comparable to that of an ITO-based device, and is suitable for TOLEDs. The voltage – current density characteristics [see Fig. 4(c)] of glass/ITO and 250 W-oxygen plasma treated glass/Ag based TOLEDs with different $5 \leq T_{Ag} \leq 9$ nm showed no severe change in the electrical properties as T_{Ag} changed. These results indicate that the glass/Ag layer that had been treated with O_2 plasma was effective as an anode because of the continuous growth of Ag film. The five types of devices had essentially no leakage current (see Fig. 4(c), inset). However, the plasma untreated glass based devices with $4 \leq T_{Ag} \leq 8$ nm did not operate because of the surface roughness of Ag film (see Fig. S7). OLEDs on the plasma-treated glass/Ag had higher current efficiency than those on glass/ITO [see Fig. 4(d)]. Although the maximum current efficiency was obtained at $T_{Ag} = 9$ nm, this may not adequate for bi-directional displays due to the preferential one-sided emission. The calculated current efficiency at 12.5 mA cm^{-2} was 40.5 cd A^{-1} on glass/ITO, but 58.68 cd A^{-1} for plasma treated glass/Ag 6 nm; this relative increase of 44.8% originates from the weak micro-cavity effect. The micro-cavity effect reduced both total internal reflection and wave-guided mode in glass and ITO, thereby increasing the luminance. Fig. S8(a) shows the normalized electroluminescence (EL) spectra of the ITO-based and $T_{Ag} = 6$ nm devices. No distinct changes were found with the ITO-based and $T_{Ag} = 6$ nm devices. Furthermore, the emission spectrum of the $T_{Ag} = 6$ nm device is independent of the viewing angle except for the case of 75° [see Fig. S8(b)]. It means that the $T_{Ag} = 6$ nm electrode did not modify the transmitted light of distort the emitted color.

3.4 FDTD Simulation

To study the effect of the weak micro-cavity structure on the electric-field distribution and the light extraction ratio of TOLEDs, 2D FDTD simulations were performed. The boundary conditions for the FDTD simulation was set to 'perfect matched layer' (PML) to avoid the occurrence of reflected electromagnetic waves at the edge of the structure. The light was considered to be emitted by excitons created in the active layer, and to have $\lambda = 510$ nm. The simulations were performed during light propagation over a distance $d = 5\,\mu$m in free space to reach steady state. A cross-sectional discrete Fourier transform monitor was used to obtain the spatial electric field distribution. Light extraction efficiency was calculated as the ratio of light output power to the power of the excitation source. The thickness of each layer was designed optically (see Fig. S9). For the ITO device, the e-field intensity of the top side was too small compared with the intensity at the bottom side. Most light escaped to the bottom side due to the reflection of the semi-transparent cathode [see Fig. 5(a)]. However, the device with $T_{Ag} = 6$ nm showed a strong e-field intensity distribution at the top side of device [see Fig. 5(c)]. Due to micro-cavity effects, the e-field intensity of top side emission increased when the Ag layer was ultra-thin [see Fig. 5(c)]. Compared to the ITO device, the electrical field distribution outside the TOLEDs was much more dynamic for the ultra-thin Ag electrode because the weak-micro cavity extracts the confined wave-guided EM wave in the ITO and organic layer [see Fig. 5(b) and (d)]. 2D-FDTD simulation (see Fig. 5(e), up) and experimental (see Fig. 5(e) down) results of extraction efficiency both indicate that the luminance of the bottom and top sides changed as a function of T_{Ag}. As T_{Ag} increased, the top side emission increased and light output obtained was identical to that of the sample with $T_{Ag} = 6$ nm (Bottom : Top = 49.6: 50.4). In order to confirm the simulation result, we fabricated and evaluated the TOLEDs with $T_{Ag} = 6$ nm. We also made the ITO device as a reference. The measured luminance of the ITO device at bottom and top sides showed large difference, the value were 1732 cd m^{-2} for top side [red dotted line in Fig. 5(e)] and 3330 cd m^{-2} for bottom side (black dotted line). Of the generated light from the active layer, 65.8% was emitted to the bottom side; this obvious asymmetric emission on the bottom side is due to reflection by the top Ag cathode. However, the TOLED with 6 nm-thick Ag film emitted almost identical luminance from both sides (bottom: 3802 cd m^{-2}, top: 3532 cd m^{-2}). In addition,

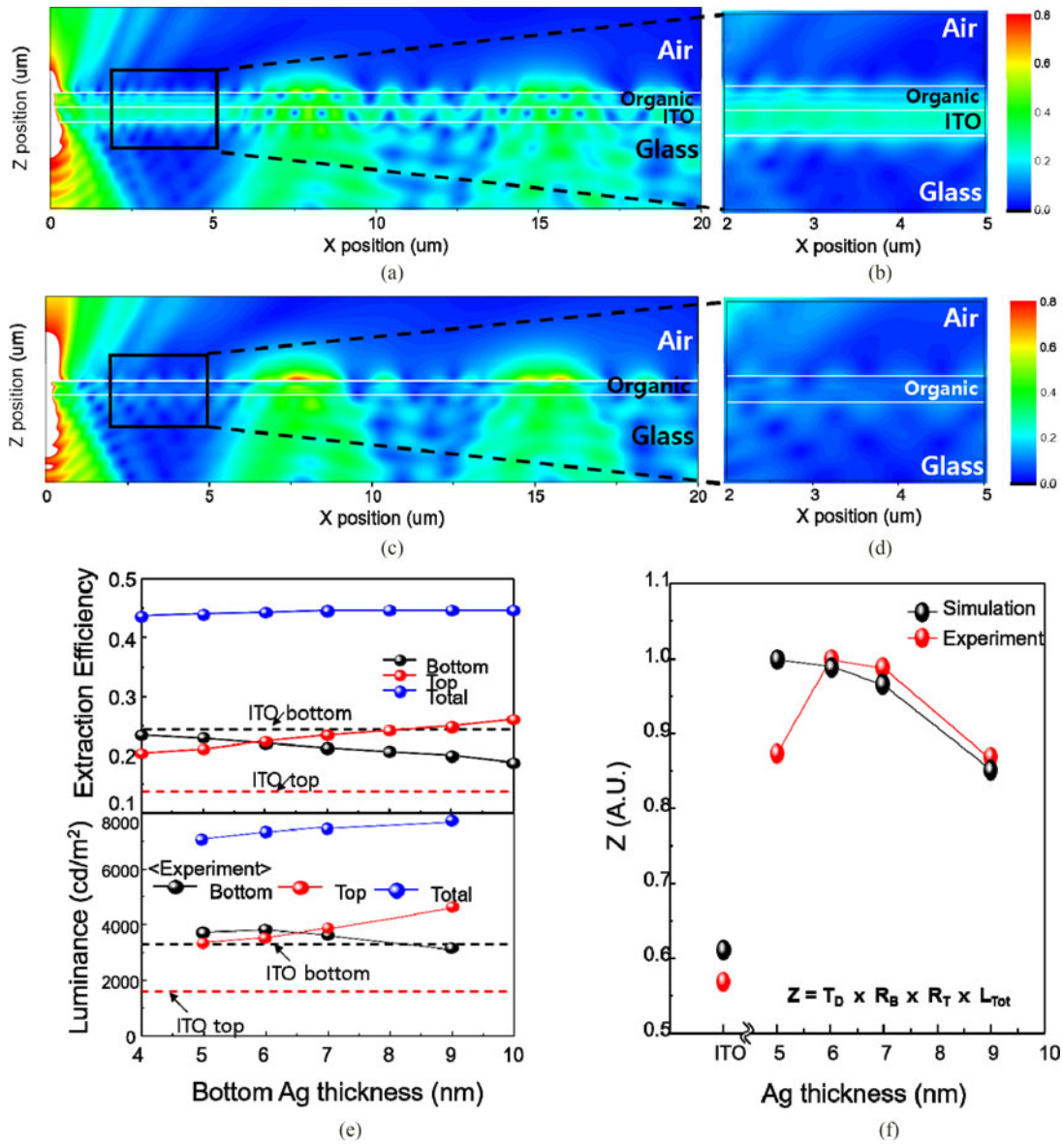

Fig. 5. Calculated electric field distribution of TOLEDs on (a,b) ITO, and (c,d) 6 nm-thick Ag electrodes with the FDTD method. (e) Calculated by FDTD values of the extraction efficiency for glass/Ag based device. (f) Figure of merit (Z) for TOLEDs as a function of Ag thickness.

due to the cavity effect, the total luminance of both side for Ag devices (7334 cd m^{-2}) could be increased compared to ITO device (5062 cd m^{-2}) by 44.8%. The figure of merit (Z) for TOLEDs was $T \times R_T \times R_B \times L_{Tot}$ [see Fig. 5(f)], where R_B is bottom side emission ratio, R_T is the total emission (R_B + top − side emission), and L_{Tot} is the normalized total luminance (maximum values of T, R_T, R_B, $L_{Tot} = 1$). The device with $T_{Ag} = 6$ nm had a high T, efficiency and symmetrical emitting structure, resulting in the highest Z value.

4. Conclusion

ITO films suffer from many problems when used as the bottom transparent electrodes in a TOLED. ITO-based TOLEDs have a preferential one-sided emission due to the difference in reflection

between the ITO and Ag electrodes. Moreover, the ITO film has a higher refractive index than the glass substrate, so light is captured in the ITO layer. The suppressing waveguide mode was demonstrated using the micro-cavity structure. Although micro-cavity effects can increase the out-coupling efficiency, the device T is degraded because of reflection by Ag. To control the micro-cavity effect to maintain device T, the thickness of the Ag layer can be decreased to $<$10 nm. However, this reduction causes new problems, because the Ag layer exhibits poor wettability on the glass substrate. This wettability can be increased by O_2 plasma treatment of the glass surface, which increases its surface energy. Due to this increased wettability of Ag, the nanoscale Ag film yields a $T \sim 76\%$ and $R_S < 10\,\Omega/\square$. The optimal anode structure for $T_{Ag} < 10$ nm is glass/Ag/WO_3 which exhibits T up to 85.6%. Fabrication of micro-cavity structures on the top of the glass/Ag/WO_3 transparent anode, yielded bottom/top emission ratio $\approx$1 for $T_{Ag} < 10$ nm. The optimized structure of TOLEDs ($T_{Ag} = 6$ nm) showed higher T (73.84%) than that of ITO (73.19%), and increased the luminance value (at 12.5 mA/cm^2) of TOLEDs by about 44.8%. We believe this proposed weak micro-cavity structure provides general guidelines for demonstrating highly transparent devices with bottom/top emission ratio $\approx$1. The design of the microcavity in the TOLED structure may significantly increase the efficiency of optoelectronic devices.

References

[1] F. Bonaccorso, Z. Sun, T. Hasan, and A. Ferrari, "Graphene photonics and optoelectronics," *Nat. Photon.*, vol. 4, no. 9, pp. 611–622, 2010.

[2] J.-H. Chang *et al.*, "Solution-processed transparent blue organic light-emitting diodes with graphene as the top cathode," *Sci. Rep.*, vol. 5, 2015, Art. no. 9693.

[3] G. Gu, V. Bulović, P. Burrows, S. Forrest, and M. Thompson, "Transparent organic light emitting devices," *Appl. Phys. Lett.*, vol. 68, no. 19, pp. 2606–2608, 1996.

[4] P. Görrn *et al.*, "Towards see-through displays: Fully transparent thin-film transistors driving transparent organic light-emitting diodes," *Adv. Mater.*, vol. 18, no. 6, pp. 738–741, 2006.

[5] S. Araki, K. Nakamura, K. Kobayashi, A. Tsuboi, and N. Kobayashi, "Electrochemical optical-modulation device with reversible transformation between transparent, mirror, and black," *Adv. Mater.*, vol. 24, no. 23, 2012, Art. no. OP122-6.

[6] G. Parthasarathy, P. Burrows, V. Khalfin, V. Kozlov, and S. Forrest, "A metal-free cathode for organic semiconductor devices," *Appl. Phys. Lett.*, vol. 72, no. 17, pp. 2138–2140, 1998.

[7] J. Meyer, P. Görrn, S. Hamwi, H.-H. Johannes, T. Riedl, and W. Kowalsky, "Indium-free transparent organic light emitting diodes with Al doped ZnO electrodes grown by atomic layer and pulsed laser deposition," *Appl. Phys. Lett.*, vol. 93, 2008, Art. no. 073308.

[8] C.-H. Chung, Y.-W. Ko, Y.-H. Kim, C.-Y. Sohn, H. Y. Chu, and J. H. Lee, "Improvement in performance of transparent organic light-emitting diodes with increasing sputtering power in the deposition of indium tin oxide cathode," *Appl. Phys. Lett.*, vol. 86, no. 9, 2005, Art. no. 093504.

[9] S. Y. Ryu, S. H. Choi, J. T. Kim, C. S. Kim, H. K. Baik, and H. S. Jeong, "Highly efficient transparent organic light-emitting diodes by ion beam assisted deposition-prepared indium tin oxide cathode," *Appl. Phys. Lett.*, vol. 90, no. 3, 2007, Art. no. 033513.

[10] J. Lee *et al.*, "Increased and balanced light emission of transparent organic light-emitting diodes by enhanced micro-cavity effects," *Opt. Lett.*, vol. 36, no. 15, pp. 2931–2933, 2011.

[11] H. Cho, J.-M. Choi, and S. Yoo, "Highly transparent organic light-emitting diodes with a metallic top electrode: The dual role of a Cs_2CO_3 layer," *Opt. Exp.*, vol. 19, no. 2, pp. 1113–1121, 2011.

[12] J. Lee *et al.*, "Systematic investigation of transparent organic light-emitting diodes depending on top metal electrode thickness," *Org. Electron.*, vol. 12, no. 8, pp. 1383–1388, 2011.

[13] C. S. Choi *et al.*, "Blur-free outcoupling enhancement in transparent organic light emitting diodes: A nanostructure extracting surface plasmon modes," *Adv. Opt. Mater.*, vol. 1, no. 10, pp. 687–691, 2013.

[14] B. Tian, G. Williams, D. Ban, and H. Aziz, "Transparent organic light-emitting devices using a MoO_3/Ag/MoO_3 cathode," *J. Appl. Phys.*, vol. 110, no. 10, 2011, Art. no. 104507.

[15] J. Lee *et al.*, "Highly efficient bi-directional organic light-emitting diodes by strong micro-cavity effects," *Appl. Phys. Lett.*, vol. 99, 2011, Art. no. 073303.

[16] J. Lee *et al.*, "Enhanced and balanced efficiency of white bi-directional organic light-emitting diodes," *Opt. Exp.*, vol. 21, no. 23, pp. 28040–28047, 2013.

[17] W. Hong Choi, H. Lam Tam, F. Zhu, D. Ma, H. Sasabe, and J. Kido, "High performance semitransparent phosphorescent white organic light emitting diodes with bi-directional and symmetrical illumination," *Appl. Phys. Lett.*, vol. 102, 2013, Art. no. 153308.

[18] W. H. Choi, H. L. Tam, D. Ma, and F. Zhu, "Emission behavior of dual-side emissive transparent white organic light-emitting diodes," *Opt. Exp.*, vol. 23, no. 11, pp. A471–A479, 2015.

[19] Y. H. Kim, J. Lee, S. Hofmann, M. C. Gather, L. Müller Meskamp, and K. Leo, "Achieving high efficiency and improved stability in ITO-free transparent organic light-emitting diodes with conductive polymer electrodes," *Adv. Funct. Mater.*, vol. 23, no. 30, pp. 3763–3769, 2013.

[20] J. Meyer *et al.*, "Transparent inverted organic light-emitting diodes with a tungsten oxide buffer layer," *Adv. Mater.*, vol. 20, no. 20, pp. 3839–3843, 2008.
[21] J.-H. Lee, S. Lee, J.-B. Kim, J. Jang, and J.-J. Kim, "A high performance transparent inverted organic light emitting diode with 1, 4, 5, 8, 9, 11-hexaazatriphenylenehexacarbonitrile as an organic buffer layer," *J. Mater. Chem.*, vol. 22, no. 30, pp. 15262–15266, 2012.
[22] J. B. Kim, J. H. Lee, C. K. Moon, S. Y. Kim, and J. J. Kim, "Highly enhanced light extraction from surface plasmonic loss minimized organic light-emitting diodes," *Adv. Mater.*, vol. 25, no. 26, pp. 3571–3577, 2013.
[23] N. Kim, H. Kang, J. H. Lee, S. Kee, S. H. Lee, and K. Lee, "Highly conductive all-plastic electrodes fabricated using a novel chemically controlled transfer-printing method," *Adv. Mater.*, vol. 27, no. 14, pp. 2317–2323, 2015.
[24] S. Höfle, A. Schienle, M. Bruns, U. Lemmer, and A. Colsmann, "Enhanced electron injection into inverted polymer light-emitting diodes by combined solution-processed zinc oxide/polyethylenimine interlayers," *Adv. Mater.*, vol. 26, no. 17, pp. 2750–2754, 2014.
[25] D. Poitras, C.-C. Kuo, and C. Py, "Design of high-contrast OLEDs with microcavity effect," *Opt. Exp.*, vol. 16, no. 11, pp. 8003–8015, 2008.
[26] I. Lee and J.-L. Lee, "Transparent electrode of nanoscale metal film for optoelectronic devices," *J. Photon. Energy*, vol. 5, no. 1, 2015, Art. no. 057609.
[27] R. Sennett and G. Scott, "The structure of evaporated metal films and their optical properties," *J. Opt. Soc. Amer.*, vol. 40, no. 4, pp. 203–211, 1950.
[28] H. Kang, S. Jung, S. Jeong, G. Kim, and K. Lee, "Polymer-metal hybrid transparent electrodes for flexible electronics," *Nat. Commun.*, vol. 6, 2015, Art. no. 6503.
[29] S. Schubert, J. Meiss, L. Müller-Meskamp, and K. Leo, "Improvement of transparent metal top electrodes for organic solar cells by introducing a high surface energy seed layer," *Adv. Energy Mater.*, vol. 3, no. 4, pp. 438–443, 2013.
[30] K. Hong, J. H. Son, S. Kim, B. H. Koo, and J.-L. Lee, "Design rules for highly transparent electrodes using dielectric constant matching of metal oxide with Ag film in optoelectronic devices," *Chem. Commun.*, vol. 48, no. 86, pp. 10606–10608, 2012.
[31] K. Hong and J.-L. Lee, "Recent developments in light extraction technologies of organic light emitting diodes," *Electron. Mater. Lett.*, vol. 7, no. 2, pp. 77–91, 2011.
[32] B. Chen, X. Sun, and S. Tan, "Transparent organic light-emitting devices with LiF/Mg: Ag cathode," *Opt. Exp.*, vol. 13, no. 3, pp. 937–941, 2005.
[33] T. Schwab *et al.*, "Highly efficient color stable inverted white top-emitting OLEDs with ultra-thin wetting layer top electrodes," *Adv. Opt. Mater.*, vol. 1, no. 10, pp. 707–713, 2013.
[34] S. Liu *et al.*, "Silver/germanium/silver: An effective transparent electrode for flexible organic light-emitting devices," *J. Mater. Chem. C*, vol. 2, no. 5, pp. 835–840, 2014.
[35] T. Schwab, S. Schubert, L. Müller-Meskamp, K. Leo, and M. C. Gather, "Eliminating micro-cavity effects in white top-emitting OLEDs by ultra-thin metallic top electrodes," *Adv. Opt. Mater.*, vol. 1, no. 12, pp. 921–925, 2013.
[36] S. Schubert, M. Hermenau, J. Meiss, L. Müller-Meskamp, and K. Leo, "Oxide sandwiched metal thin-film electrodes for long-term stable organic solar cells," *Adv. Funct. Mater.*, vol. 22, no. 23, pp. 4993–4999, 2012.
[37] B. K. Kim, Y. H. Cho, B. T. Ahn, and D. G. Moon, "Structural characterization of the Ag/Ca transparent electrode for organic light emitting diodes," *Electron. Mater. Lett.*, vol. 4, no. 1, pp. 19–24, 2008.
[38] G. Gu, D. Garbuzov, P. Burrows, S. Venkatesh, S. Forrest, and M. Thompson, "High-external-quantum-efficiency organic light-emitting devices," *Opt. Lett.*, vol. 22, no. 6, pp. 396–398, 1997.
[39] W. Zhang, H. Liu, and R. Sun, "Full color organic light-emitting devices with microcavity structure and color filter," *Opt. Exp.*, vol. 17, no. 10, pp. 8005–8011, 2009.
[40] L. Gerenser, "Photoemission investigation of silver/poly (ethylene terephthalate) interfacial chemistry: The effect of oxygen-plasma treatment," *J. Vac. Sci. Technol. A, Vac. Surf. Films*, vol. 8, no. 5, pp. 3682–3691, 1990.
[41] S. Y. Kim, K. Hong, K. Kim, H. K. Yu, W.-K. Kim, and J.-L. Lee, "Effect of N_2, Ar, and O_2 plasma treatments on surface properties of metals," *J. Appl. Phys.*, vol. 103, 2008, Art. no. 076101.
[42] N. Formica, D. S. Ghosh, A. Carrilero, T. L. Chen, R. E. Simpson, and V. Pruneri, "Ultrastable and atomically smooth ultrathin silver films grown on a copper seed layer," *ACS Appl. Mater. Interfaces*, vol. 5, no. 8, pp. 3048–3053, 2013.
[43] K. Hong *et al.*, "Optical properties of WO_3/Ag/WO_3 multilayer as transparent cathode in top-emitting organic light emitting diodes," *J. Phys. Chem. C*, vol. 115, no. 8, pp. 3453–3459, 2011.
[44] C. Zhang *et al.*, "An ultrathin, smooth, and low-loss Al-doped Ag film and its application as a transparent electrode in organic photovoltaics," *Adv. Mater.*, vol. 26, no. 32, pp. 5696–5701, 2014.
[45] H. Cho, C. Yun, and S. Yoo, "Multilayer transparent electrode for organic light-emitting diodes: Tuning its optical characteristics," *Opt. Exp.*, vol. 18, no. 4, pp. 3404–3414, 2010.